IEEE Access
Multidisciplinary | Rapid Review | Open Access Journal

SPECIAL SECTION ON ADVANCED ENERGY STORAGE TECHNOLOGIES AND THEIR APPLICATIONS

Received June 1, 2019, accepted June 19, 2019, date of publication July 8, 2019, date of current version August 28, 2019.

Digital Object Identifier 10.1109/ACCESS.2019.2927416

Minimum Copper Loss Direct Torque Control of Brushless DC Motor Drive in Electric and Hybrid Electric Vehicles

QINGCHAO ZHANG[1], JUNJUN DENG[2], (Member, IEEE), AND NA FU[2]
[1]Shenyang Aircraft Design and Research Institute, Shenyang 110035, China
[2]National Engineering Laboratory for Electric Vehicles, Beijing Institute of Technology, Beijing 100081, China

Corresponding author: Junjun Deng (dengjunjun@bit.edu.cn)

This work was supported by the National Natural Science Foundation of China under Grant 51707010.

ABSTRACT A novel direct torque control (DTC) method with copper loss minimization is proposed for the brushless dc motor (BLDCM) in electric vehicle (EV) application. In order to realize high efficiency and high torque control precision at the same time, a special stator flux linkage trajectory is designed based on pseudo-dq transformation for maximum torque per ampere (MTPA) control of BLDCM. The three-phase conduction voltage vectors switch table is used to realize the flux linkage tracking control for high dynamic performance of torque control. The torque ripple caused by the non-ideality of the back EMF and the commutation in traditional two-phase conduction voltage vector based DTC method can be eliminated, which improves the torque control precision. The validity and effectiveness of the proposed DTC scheme are verified through experimental results.

INDEX TERMS Brushless dc motor (BLDCM), direct torque control (DTC), maximum torque per ampere (MTPA), minimum copper loss, stator flux linkage control.

I. INTRODUCTION

Brushless dc motor (BLDCM) has been widely used in aviation, electric vehicles, flywheel-based energy storage system and other industrial uses, due to its advantages such as simple structure, high power density, and high efficiency. The BLDCM with trapezoidal back electromotive force (EMF) and the popular used permanent magnet synchronous motor (PMSM) with sinusoidal back EMF are two kinds of permanent magnet motors with high similarity in structure and property. It is shown in [1] that the BLDCM drive system has higher power propulsion capability than the PMSM drive system. However, limited by traditional control methods, the potential performance of BLDCM has not been excavated.

The traditional BLDCM double closed loop control system adopting the two-phase conduction mode, which is based on the three-phase-six-state PWM control scheme, neglects the dynamic process of motor commutation and regards the back EMF as the ideal trapezoidal waveform, which leads to the torque ripple caused by both the non-ideality of the back EMF and the commutation. Besides, high torque is required by the motor drive system in the heavy duty applications. It usually means high winding current, which leads to an increase in the copper loss and a decrease in the drive system efficiency. Therefore, the maximum torque per ampere (MTPA) control is usually adopted to minimize copper loss and improve motor efficiency. Meanwhile, torque ripple suppression is equally important for the BLDCM drive system to be applied in the EV application that calls for high precision and high efficiency at the same time.

Substantial efforts have been directed to reducing the torque ripple of BLDCM, and result in a rich library of related literature. Direct torque control (DTC) technique, which was originally proposed by Takahashi and Noguchi [2] and Depenbrock [3] for induction motor drives, has been extended to BLDCM drives [4]–[6], which can reduce the torque ripple and achieve higher dynamic performance compared with the traditional vector control based on proportional-integral (PI) control. There have been three typical BLDCM-DTC schemes presented in [4]–[6], including DTC with constant flux linkage amplitude control, DTC without flux linkage control and DTC with indirect flux linkage control. In the first two schemes, two-phase conduction voltage space vectors

The associate editor coordinating the review of this article and approving it for publication was Rui Xiong.

are defined and used. However, it has been concluded that the commutation torque ripple cannot be eliminated when the BLDCM runs at high speed in the two-phase conduction mode [7].

In order to reduce the commutation torque ripple, a hybrid mode, which brings in the three-phase switching mode only during the commutation, has been proposed in [7]. In the DTC scheme with indirect flux linkage control, three-phase conduction voltage space vectors are adopted. Moreover, a hybridization control in two-phase conduction mode with the integration of the methods presented in [7] and [8] is proposed in [9]. Furthermore, to suppress the commutation torque ripple, the combined two-and-three phase conduction DTC of BLDCM with overlap angle control is proposed [10]. The optimum commutation overlap angle is determined with respect to load and speed. In [11], torque ripple is reduced by using a three-level hysteresis torque controller. The average switching frequencies of the upper and lower bridge arm of the inverter turn to be balanced. For reducing the torque ripple resulting from chopped wave further while maintaining constant switching frequency, a novel DTC method is proposed in [12] by introducing an optimized duty ratio control to conventional hysteresis based DTC.

Although many different DTC method with various advantages have been studied in [4]–[12], the flux linkage control has not been considered. Therefore, the more advanced strategies such as flux-weakening control and copper loss minimization control, cannot be realized. Particularly, an indirect stator flux linkage control is performed by controlling the flux related d-axis current using hysteresis control in [6], in which the DTC of BLDCM is achieved on the basis of classical dq transformation and three-phase conduction voltage space vectors. Thus, the torque ripple is reduced effectively, and the BLDCM could operate in the flux-weakening region by properly selecting the d-axis current reference. However, in the above mentioned DTC schemes, the MTPA control is not considered. In classical dq reference frame, the d-axis back EMF of BLDCM is not zero since the back EMF of BLDCM is trapezoidal. Electromagnetic torque is related to both d-axis current and q-axis current. The MTPA control cannot be achieved by making d-axis current zero. Therefore, the torque-to-current ratio for BLDCM needs to be further optimized.

A vector control method based on the pseudo-dq transformation of BLDCM for realizing the MTPA control and reducing the torque ripple is proposed in [13]. After the coordinate transformation, the d-axis back EMF waveform function is zero, and the electromagnetic torque is only related to the q-axis back EMF waveform function and the q-axis current. The MTPA control can be achieved by making the d-axis current zero. It is theoretically proved in [14] that the vector control based on the pseudo-dq transformation holds the advantages of lower torque ripple and lower copper loss.

In this study, a novel DTC method for BLDCM is proposed using direct stator flux linkage trajectory tracking technique, which is suitable for MPTA operations. Compared with the previous two-phase conduction based DTC schemes without flux linkage control and the indirect flux control DTC technique, the proposed DTC method differs on its direct stator flux linkage trajectory closed loop control. The stator flux linkage trajectory reference is designed based on the principle of BLDCM-MTPA control. Besides, the presented method uses pseudo-dq coordinate transformation and three-phase conduction voltage vectors for DTC realization. In this case, both the torque and the flux linkage of BLDCM are controlled directly and simultaneously, which enables the torque ripple eliminating operation as well as MTPA control. The voltage vectors of the proposed DTC method are directly generated from a simple look-up table depending on the outputs of hysteresis torque and direct flux linkage comparators. The overall control is much simpler while a faster torque response can be achieved compared to the conventional PI control algorithm based PWM control techniques.

This paper presents a novel direct torque and direct flux linkage control of BLDCM. Pseudo-dq transformation proposed in [13] is extended to design the stator flux linkage trajectory reference. Three-phase conduction voltage vectors are used to control both the torque and the flux linkage simultaneously. The rest of the paper is organized as follows. The Pseudo-dq(DQ) transformation and MTPA electromagnetic torque control is introduced. The principle of MTPA stator flux linkage trajectory control method is elaborated. Experimental results are presented to illustrate the validity and effectiveness of the proposed BLDCM-MTPA-DTC scheme on minimizing the torque ripple and the copper loss.

II. MTPA STATOR FLUX LINKAGE TRACKING DTC OF BLDCM

A. PSEUDO-DQ(DQ) TRANSFORMATION AND MTPA ELECTROMAGNETIC TORQUE CONTROL

In classical dq reference frame, the electromagnetic torque of trapezoidal waveform back EMF BLDCM and sinusoidal waveform back EMF PMSM can be expressed as

$$T_e = n_p k_e \left[f_d(\theta_r) i_d + f_q(\theta_r) i_q \right] \tag{1}$$

where the $f_d(\theta_r), f_q(\theta_r)$, i_d and i_q are the back EMF waveform functions and stator currents in the d- and q-axis, respectively, and n_p is the number of pole-pairs, k_e is the phase back EMF constant, θ_r is the electrical rotor angular position in dq reference frame.

For PMSM with sinusoidal waveform back EMFs, $f_d(\theta_r) = 0$, i_d makes no contributions to generate T_e , T_e is simplified to

$$T_e = n_p k_e f_q(\theta_r) i_q \tag{2}$$

where the $f_q(\theta_r)$ is constant. Obviously, the $i_d = 0$ control is just the MTPA control of PMSM.

But, for BLDCM with trapezoidal waveform back EMFs, $f_d(\theta_r) \neq 0$, T_e cannot be simplified to (2),$i_d = 0$ control is not the MTPA control.

The pseudo-dq transformation theory is proposed for non-sinusoidal waveform PMSM vector control in [5].

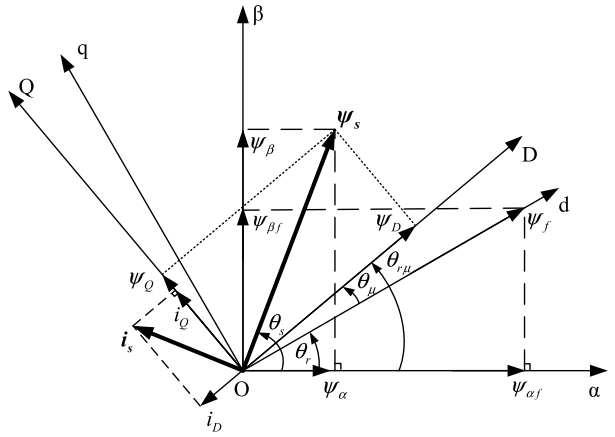

FIGURE 1. Rotor and stator flux linkages of a BLDCM in the stationary $\alpha\beta$-plane, dq-plane, and DQ-plane.

It is also practicable for BLDCM or PMSM with any pattern of back EMFs. With this transformation, the electromagnetic torque expression can be simplified to the form of (2), then, the high dynamic performance vector control with minimizing torque ripple and copper loss can be achieved.

In order to distinguish the pseudo-dq reference frame and the classical dq reference frame clearly, pseudo-dq is denoted as DQ in writing in this paper. The stationary $\alpha\beta$ reference frame, classical dq reference frame, and the DQ reference frame are shown in Figure 1, where $\boldsymbol{\psi}_s$ is the stator flux vector, ψ_f is the rotor flux generated by the permanent magnet, and $\boldsymbol{i}_s$ is the stator current. According to Figure 1, the coordinate transformation matrix between the DQ reference frame and the $\alpha\beta$ reference frame can be obtained as

$$\mathbf{C}_{\mathbf{DQ2}\boldsymbol{\alpha\beta}} = \begin{bmatrix} \cos(\theta_r + \theta_\mu) & -\sin(\theta_r + \theta_\mu) \\ \sin(\theta_r + \theta_\mu) & \cos(\theta_r + \theta_\mu) \end{bmatrix} \tag{3}$$

where θ_r is the rotor position angle of BLDCM, and θ_μ is the angle between the D-axis and the d-axis.

The electromagnetic torque T_e of a BLDCM with non-ideal trapezoidal back EMF waveform can be expressed in the rotary DQ reference frame as

$$T_e = n_p k_e \left[f_D(\theta_{r\mu}) i_D + f_Q(\theta_{r\mu}) i_Q \right] \tag{4}$$

where the $f_D(\theta_{r\mu})$, $f_Q(\theta_{r\mu})$, i_D and i_Q are the back EMF waveform functions and stator currents in the D- and Q-axis, respectively, and $\theta_{r\mu}$ is the electrical rotor angular position in DQ reference frame, $\theta_{r\mu} = \theta_r + \theta_\mu$.

With DQ transformation, the $f_D(\theta_{r\mu})$ is forced to 0, then i_D makes no contributions to generate T_e, thus, the $i_D = 0$ control is just the MTPA control, and the T_e can be simplified as

$$T_e = n_p k_e f_Q(\theta_{r\mu}) i_Q \tag{5}$$

which is nearly the same as the expression of (2), except that $f_Q(\theta_{r\mu})$ is not a constant, it depends on the angle $\theta_{r\mu}$.

To obtain $f_D(\theta_{r\mu}) = 0$, it would be necessary to have the following

$$\begin{aligned} \begin{bmatrix} f_\alpha(\theta_r) \\ f_\beta(\theta_r) \end{bmatrix} &= \mathbf{C}_{\mathbf{DQ2}\boldsymbol{\alpha\beta}} \begin{bmatrix} f_D(\theta_{r\mu}) \\ f_Q(\theta_{r\mu}) \end{bmatrix} \\ &= \begin{bmatrix} \cos(\theta_r + \theta_\mu) & -\sin(\theta_r + \theta_\mu) \\ \sin(\theta_r + \theta_\mu) & \cos(\theta_r + \theta_\mu) \end{bmatrix} \begin{bmatrix} 0 \\ f_Q(\theta_{r\mu}) \end{bmatrix} \end{aligned} \tag{6}$$

where the $f_\alpha(\theta_r), f_\beta(\theta_r)$ are the back EMF waveform functions in the α- and β-axis.

By solving the equations of (6), θ_μ and $f_Q(\theta_{r\mu})$ can be obtained as

$$\begin{cases} \theta_\mu = arc\tan\left(-\dfrac{f_\alpha(\theta_r)}{f_\beta(\theta_r)} \right) - \theta_r \\ f_Q(\theta_{r\mu}) = \sqrt{f_\alpha^2(\theta_r) + f_\beta^2(\theta_r)} \end{cases} \tag{7}$$

B. MTPA STATOR FLUX LINKAGE TRAJECTORY CONTROL

For BLDCM with surface-mounted permanent magnet rotor, the stator flux linkage equations in stationary $\alpha\beta$ reference frame can be written as

$$\begin{cases} \psi_\alpha = L_M i_\alpha + \psi_{\alpha f}(\theta_r) \\ \psi_\beta = L_M i_\beta + \psi_{\beta f}(\theta_r) \end{cases} \tag{8}$$

where ψ_α, ψ_β, i_α, i_β, $\psi_{\alpha f}(\theta_r)$ and $\psi_{\beta f}(\theta_r)$ are the stator flux linkages, stator currents, and rotor flux linkages in α- and β-axis, respectively, the L_M is the phase equivalent inductance.

The magnitude and angular position of the stator flux linkage vector is obtained as

$$\begin{cases} \psi_s = \sqrt{\psi_\alpha^2 + \psi_\beta^2} \\ \theta_s = \arctan\left(\dfrac{\psi_\beta}{\psi_\alpha} \right) \end{cases} \tag{9}$$

Assume T_e^* is the reference torque, the Q-axis reference current i_Q^* can be obtained from (5) as

$$i_Q^* = \frac{T_e^*}{n_p k_e f_Q(\theta_{r\mu})} \tag{10}$$

Applying the coordinate transformation between the DQ reference frame and the $\alpha\beta$ reference frame in (10), the reference current i_α^*, i_β^* can be expressed as

$$\begin{bmatrix} i_\alpha^* \\ i_\beta^* \end{bmatrix} = \mathbf{C}_{\mathbf{DQ2}\boldsymbol{\alpha\beta}} \begin{bmatrix} i_D^* \\ i_Q^* \end{bmatrix} = \mathbf{C}_{\mathbf{DQ2}\boldsymbol{\alpha\beta}} \begin{bmatrix} 0 \\ i_Q^* \end{bmatrix} \tag{11}$$

On the basis of (8) - (11), the MTPA stator flux linkage trajectory reference ψ_s^* can be designed as

$$\psi_s^* = \sqrt{\psi_\alpha^{*2} + \psi_\beta^{*2}} \tag{12}$$

where

$$\begin{cases} \psi_\alpha^* = L_M i_\alpha^* + \psi_{\alpha f}(\theta_r) \\ \psi_\beta^* = L_M i_\beta^* + \psi_{\beta f}(\theta_r) \end{cases}$$

The proposed BLDCM-MTPA-DTC scheme is shown in Figure 2.

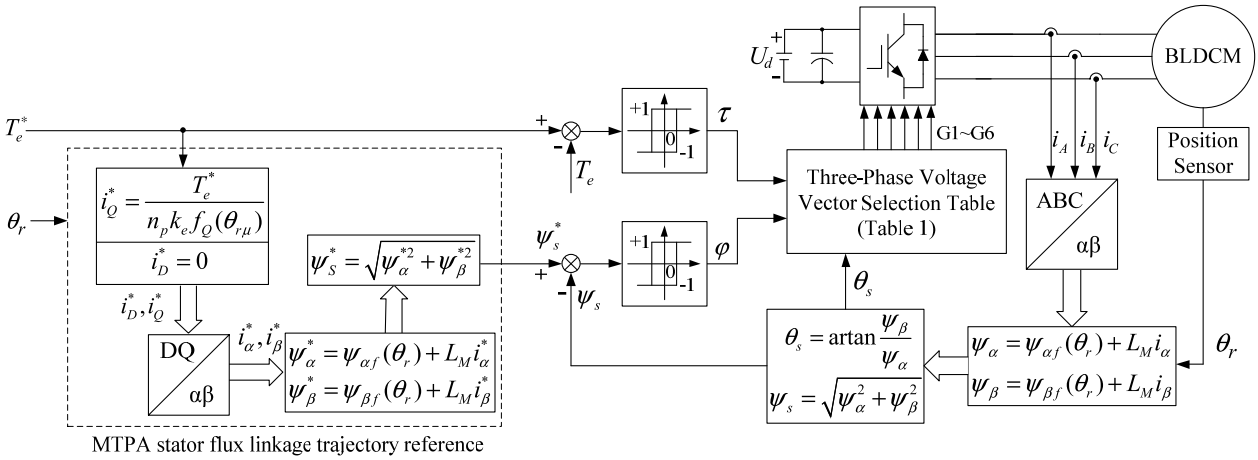

FIGURE 2. Overall block diagram of the MTPA-DTC of BLDCM drive using three-phase conduction mode.

TABLE 1. Units for magnetic properties.

φ	τ	Sector I	II	III	IV	V	VI
1	1	$\mathbf{u}_{S2}$	$\mathbf{u}_{S3}$	$\mathbf{u}_{S4}$	$\mathbf{u}_{S5}$	$\mathbf{u}_{S6}$	$\mathbf{u}_{S1}$
1	-1	$\mathbf{u}_{S6}$	$\mathbf{u}_{S1}$	$\mathbf{u}_{S2}$	$\mathbf{u}_{S3}$	$\mathbf{u}_{S4}$	$\mathbf{u}_{S5}$
-1	1	$\mathbf{u}_{S3}$	$\mathbf{u}_{S4}$	$\mathbf{u}_{S5}$	$\mathbf{u}_{S6}$	$\mathbf{u}_{S1}$	$\mathbf{u}_{S2}$
-1	-1	$\mathbf{u}_{S5}$	$\mathbf{u}_{S6}$	$\mathbf{u}_{S1}$	$\mathbf{u}_{S2}$	$\mathbf{u}_{S3}$	$\mathbf{u}_{S4}$

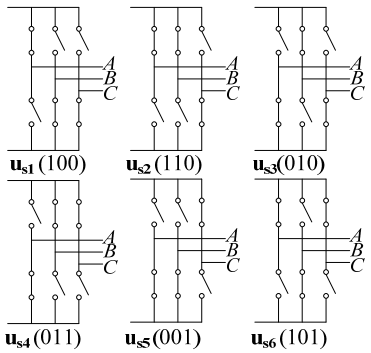

FIGURE 3. Nonzero voltage space vectors for BLDCM-MTPA-DTC drive.

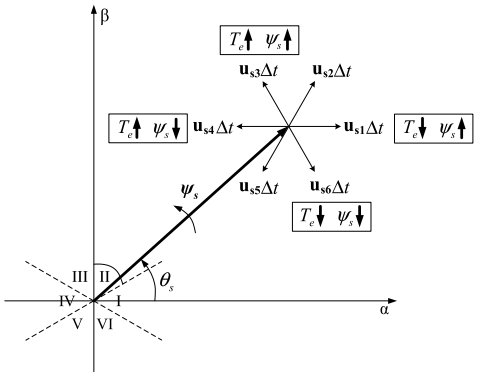

FIGURE 4. Stator voltage vector selection and its control on flux linkage and torque (sector II).

For controlling both the stator flux linkage trajectory and the torque, six nonzero voltage space vectors are defined as shown in Figure 3, and the switching table given in Table 1.

In Table 1, φ is the output of flux linkage hysteresis comparator, τ is the output of torque hysteresis comparator, and the flux linkage sector is denoted as I, II, III, IV, V, VI. For both φ and τ, 1 means that the actual value is below the reference and -1 means that the actual value exceeds the reference. According to the output of the hysteresis comparator and the flux linkage sector, the stator voltage vector can be selected, so that the error values of the flux linkage and the torque are controlled within the hysteresis range.

The basic considerations of selecting the stator voltage vector $\mathbf{u_s}$ for the BLDCM-MTPA-DTC includes: 1) the control of stator flux amplitude by the radial component of $\mathbf{u_s}$; 2) the control of rotational speed by the tangential component of $\mathbf{u_s}$. Taking the flux linkage sector II as an example, the control effect of the non-zero voltage vector on the flux linkage and torque is shown in Figure 4.

Since the back-EMF of BLDCM is trapezoidal, the stator flux linkage trajectory is not pure circle as in PMSM whose back-EMF is sinusoidal. The MTPA stator flux linkage trajectory of BLDCM is more like a hexagonal shape or six petals shape as shown in Figure 5. Actually, the flux linkage trajectory tends to be circular with the shape of the back-EMF tending to be sinusoidal.

Figure 5 shows how to select the vector voltage from the switch table to limit the amplitude of the flux linkage to a

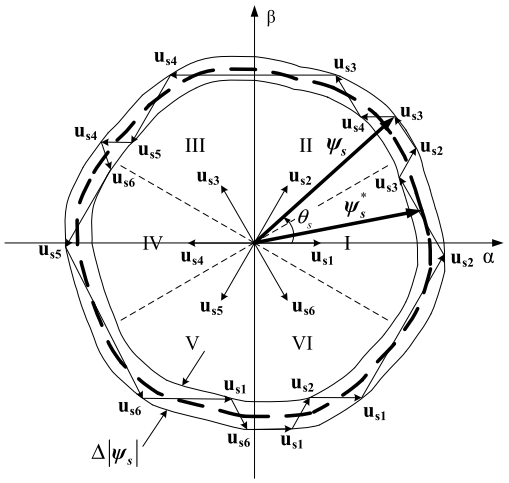

FIGURE 5. MTPA stator flux linkage trajectory of BLDCM in the stationary $\alpha\beta$–plane.

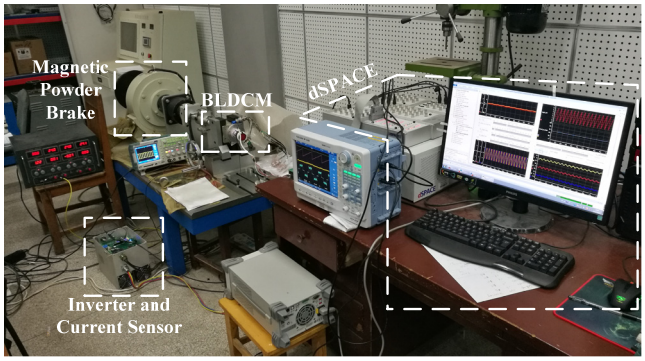

FIGURE 6. Experimental test-bed.

TABLE 2. Parameters of the test BLDCM.

Symbol	Parameter	Value
L_M	Equivalent winding inductance(mH)	2
R	Winding resistance(Ω)	0.3
K_e	Phase back EMF constant	0.06
n_p	(V/(rad·s-1))	2

hysteresis band of a given value, assuming τ is always 1. It can be seen from Fig. 5 that the terminal of the flux linkage ψ_s moves along the direction of the applied voltage vector and remains in the hysteresis band at all times.

III. EXPERIMENT RESULTS

The proposed BLDCM-MTPA-DTC scheme shown in Figure 2 has been achieved with the experimental test-bed shown in Figure 6. The specific DTC algorithm is implemented by using the dSPACE system. The sampling interval is 20 μs. The magnitudes of the torque and flux linkage hysteresis bands are 0.001N·m and 0.001Wb, respectively. The main parameters of the BLDCM using in the experiment are given in Table 2. The DC-link voltage U_d is 30V.

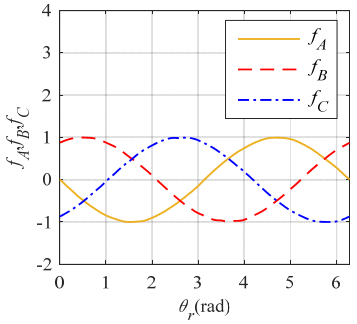

FIGURE 7. Actual ABC-axis normalized non-ideal trapezoidal waveform phase back EMF waveform functions versus electrical rotor position.

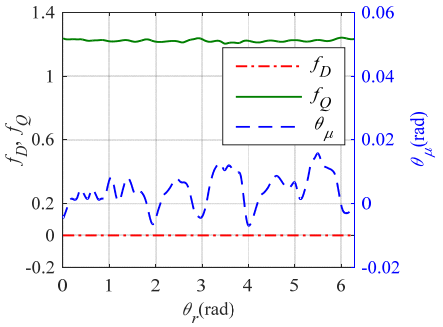

FIGURE 8. Actual D- and Q-axis back EMF waveform functions and angle θ_μ versus electrical rotor position.

Figure 7 shows the ABC frame back EMF waveform functions versus electrical rotor position of the BLDCM in the experiment. The waveforms look like a sine wave, but they are not purely sinusoidal, this can be proved by Figure 8. Figure 8 shows the transformed DQ frame back EMF waveform functions and the angle θ_μ between dq frame and DQ frame versus electrical rotor position θ_r. According to the DQ (pseudo-dq) transformation theory, it can be verified that, in the sine wave case, $\theta_\mu = 0$ and $f_Q(\theta_{r\mu})$ would be a constant which equals to $f_q(\theta_r)$ in dq frame.

As shown in (7) and Figure 8, in DQ frame the θ_μ and $f_Q(\theta_{r\mu})$ are functions depending on θ_r, they are set up in the look-up tables for torque calculation and stator flux linkage reference design in the experiment.

For the BLDCM with trapezoidal waveform phase back EMFs, its MTPA stator flux linkage trajectory should be hexagonal shape or six petals shape as shown in Figure 5, but it tends to be circular along with the shape of the back-EMF waveforms tending to be sinusoidal, thereby, with the back-EMF waveforms shown in Figure 7, experimental MTPA stator flux linkage trajectories at 0.7N·m and 2N·m load torque appear as Figure 9. The relationship between the stator flux linkage trajectory and back-EMF waveforms is not the focus of this paper, it is left as a future research study.

In the experimental test, the BLDCM drive system is designed to be a speed-torque dual closed-loop structure.

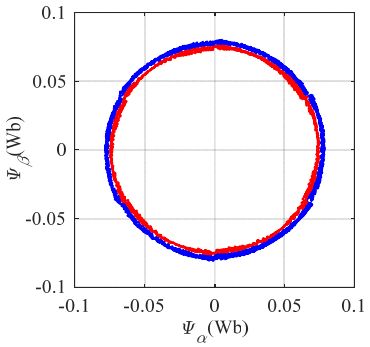

FIGURE 9. Experimental MTPA stator flux linkage trajectories under the three-phase conduction DTC of BLDCM drive at 0.7N·m (inner trajectory) and 2N·m(outer trajectory) load torque.

Reference torque T_e^* is the output of the speed PI regulator. Figure 10 and Figure 11 show the response waveforms of electromagnetic torque, mechanical angular speed, D- and Q-axis currents and copper loss, respectively, under a 0.7N·m load torque condition.

The results shown in Figure 10 are obtained by using the proposed BLDCM-MTPA-DTC method. The results shown in Figure 11 are obtained by using the BLDCM-DTC method without flux linkage control based on traditional two-phase conduction voltage vector.

According to the study in [6], the commutation torque ripples will occur at high speed when the DTC method based on two-phase conduction voltage space vectors is used. While 25% of the DC-link voltage is the back EMF amplitude demarcation point between the low speed and the high speed defined in [6]. In this experiment, 62.5rad/s is the computed initial point of high speed at which the back EMF amplitude reaches 25% of the DC-link voltage (30V) in this experiment.

It is seen in Figure 10(a) and Figure 10(b) that, under the proposed DTC method in this paper, fast response of the electromagnetic torque is obtained and the electromagnetic torque tracks the reference torque closely even at high speed over 62.5rad/s. The electromagnetic torque is quite well controlled with inevitable but acceptable torque ripples resulting from power switches chopping.

It is seen in Figure 11(a) and Figure 11(b) that, under the BLDCM-DTC method without flux linkage control, fast response of the electromagnetic torque is obtained, but the commutation torque ripple occurs at high speed over 62.5rad/s. Because the actual back EMF waveform functions are considered in the experiment, the torque ripple resulting from the non-ideality of the back EMF does not appears in Figure 11(a) and Figure 11(b).

Considering (5), the electromagnetic torque is totally generated by Q-axis current, the D-axis current makes no contributions to generate. It is seen in Figure 10(c) that the D-axis current oscillates around the desired zero reference value, which means that the MTPA control (or copper loss minimization control) is realized. While the D-axis current

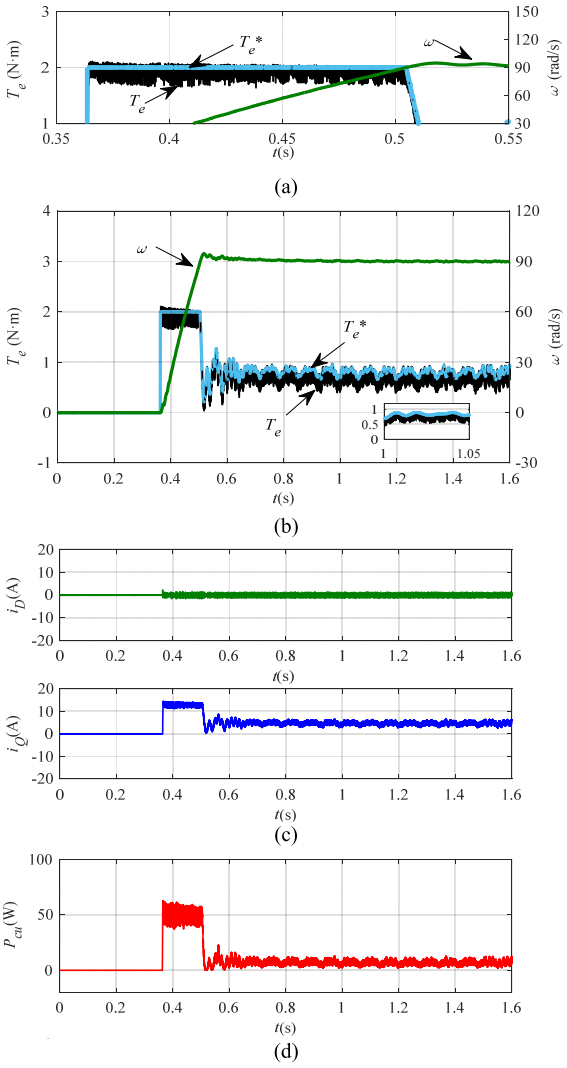

FIGURE 10. Steady-state and transient behavior of the BLDCM-MTPA-DTC experiment. (a) Partial enlarged detail of (b). (b) Referenced electromagnetic torque T_e^*, actual electromagnetic torque T_e and mechanical angular speed ω. (c) D-axis stator current and Q-axis stator current. (d) Copper loss.

shown in Figure 11(c) is not zero, the D-axis current is wasted for generating additional copper loss, this means that the MTPA control (or copper loss minimization control) cannot be realized by using the BLDCM-DTC method without flux linkage control.

It is known from Figure 10(c), Figure 10(d), Figure 11(c) and Figure 11(d), the copper loss increase with electromagnetic torque. Obviously, minimizing copper loss is beneficial and important for improving the BLDCM's operating efficiency under high torque and high load.

Figure 12 shows the comparison result of copper loss between the BLDCM-MTPA-DTC method and the BLDCM-DTC without flux linkage control method. Pcu2 and Pcu1 are the copper loss under the BLDCM-MTPA-DTC and the BLDCM-DTC method without flux linkage

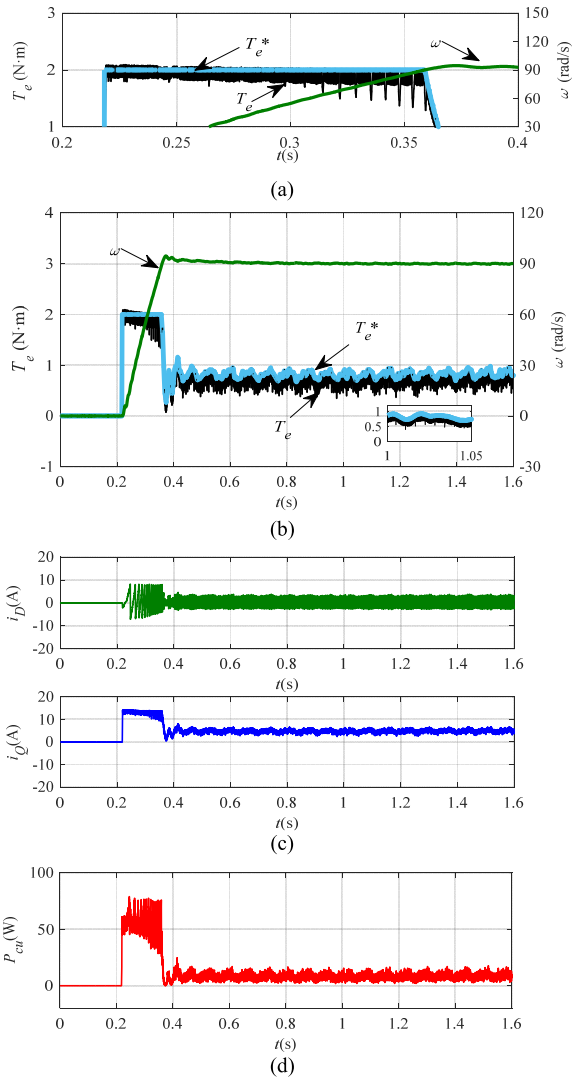

FIGURE 11. Steady-state and transient behavior of the BLDCM-DTC experiment without flux linkage control based on traditional two-phase conduction voltage vector. (a) Partial enlarged detail of (b). (b) Referenced electromagnetic torque T_e^*, actual electromagnetic torque T_e, and mechanical angular speed ω. (c) D-axis stator current and Q-axis stator current. (d) Copper loss.

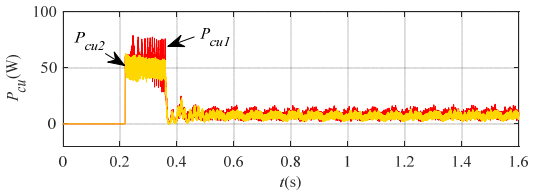

FIGURE 12. Copper loss under the BLDCM-MTPA-DTC method (Pcu2) and the copper loss under the BLDCM-DTC method without flux linkage control (P_{cu1}).

control respectively. Obviously, Pcu2 is less than Pcu1, especially under high torque and high load.

IV. CONCLUSION

In this paper, MTPA control based on pseudo-dq transformation has been successfully applied to the direct stator flux linkage close loop control of BLDCM. The using of pseudo-dq transformation and the actual back EMF waveform functions makes the presented DTC scheme can be used for various BLDCMs with non-ideal trapezoidal waveform back EMFs. It is shown that, with the proposed DTC scheme, direct torque control and direct flux linkage control of BLDCM can be implemented simultaneously, both the torque ripple resulting from the non-ideality of the back EMFs and the commutation torque ripple occurring at high speed in the traditional two-phase conduction voltage vector based DTC method are eliminated. The presented control method improves the BLDCM performance in the aspects of torque control precision and copper loss reduction, which makes it feasible for the EV application.

ACKNOWLEDGMENT

The authors would like to thank Yigeng Huangfu of Northwestern Polytechnical University for his assistance in experimental equipment.

REFERENCES

[1] A. Lidozzi, L. Solero, F. Crescimbini, and R. Burgos, "Vector control of trapezoidal back-EMF PM machines using pseudo-Park transformation," in *Proc. IEEE Power Electron. Spec. Conf.*, Rhodes, Greece, Jun. 2008, pp. 2167–2171.
[2] I. Takahashi and T. Noguchi, "A new quick-response and high-efficiency control strategy of an induction motor," *IEEE Trans. Ind. Appl.*, vol. IA-22, no. 5, pp. 820–827, Sep. 1986.
[3] M. Depenbrock, "Direct self-control (DSC) of inverter-fed induction machine," *IEEE Trans. Power Electron.*, vol. 3, no. 4, pp. 420–429, Oct. 1988.
[4] Y. Liu, Z. Q. Zhu, and D. Howe, "Direct torque control of brushless DC drives with reduced torque ripple," *IEEE Trans. Ind. Appl.*, vol. 41, no. 2, pp. 599–608, Mar. 2005.
[5] S. B. Ozturk and H. A. Toliyat, "Direct torque control of brushless DC motor with non-sinusoidal back-EMF," in *Proc. IEEE Int. Electr. Mach. Drives Conf.*, Mar. 2007, pp. 165–171.
[6] S. B. Ozturk and H. A. Toliyat, "Direct torque and indirect flux control of brushless DC motor," *IEEE/ASME Trans. Mechatron.*, vol. 16, no. 2, pp. 351–360, Apr. 2011.
[7] Y. Liu, Z. Q. Zhu, and D. Howe, "Commutation-torque-ripple minimization in direct-torque-controlled PM brushless DC drives," *IEEE Trans. Ind. Appl.*, vol. 43, no. 4, pp. 1012–1021, Jul. 2007.
[8] K.-Y. Nam, W.-T. Lee, C.-M. Lee, and J.-P. Hong, "Reducing torque ripple of brushless DC motor by varying input voltage," *IEEE Trans. Magn.*, vol. 42, no. 4, pp. 1307–1310, Apr. 2006.
[9] S. A. K. H. M. Niapour, M. Tabarraie, and M. R. Feyzi, "A new robust speed-sensorless control strategy for high-performance brushless DC motor drives with reduced torque ripple," *Control Eng. Pract.*, vol. 24, pp. 42–54, Mar. 2014.
[10] C. K. Lad and R. Chudamani, "A simple overlap angle control strategy for reducing commutation torque ripple in a brushless DC motor drive," *Eng. Sci. Technol., Int. J.*, vol. 20, no. 4, pp. 1406–1419, Apr. 2017.
[11] M. Masmoudi, B. El Badsi, and A. Masmoudi, "Direct torque control of brushless DC motor drives with improved reliability," *IEEE Trans. Ind. Appl.*, vol. 50, no. 6, pp. 3744–3753, Nov. 2014.
[12] H. Liu and H. Zhang, "A novel direct torque control method for brushless DC motors based on duty ratio control," *J. Franklin Inst.*, vol. 354, no. 10, pp. 4055–4072, Jul. 2017.
[13] D. Grenier and J.-P. Louis, "Use of an extension of the park's transformation to determine control laws applied to a non-sinusoidal permanent magnet synchronous motor," in *Proc. 5th Eur. Conf. Power Electron. Appl.*, Sep. 1993, pp. 32–37.
[14] P. Kshirsagar and R. Krishnan, "High-efficiency current excitation strategy for variable-speed nonsinusoidal back-EMF PMSM machines," *IEEE Trans. Ind. Appl.*, vol. 48, no. 6, pp. 1875–1889, Nov./Dec. 2012.

QINGCHAO ZHANG received the B.S., M.S., and Ph.D. degrees in electrical engineering from Northwestern Polytechnical University, Xi'an, China, in 2008, 2011, and 2017, respectively. Since August 2017, he has been with the Shenyang Aircraft Design and Research Institute, Shenyang, China, where he is currently an Engineer. His research interests include electrical machines control, power electronics, and electric drive.

JUNJUN DENG received the B.S., M.S., and Ph.D. degrees in electrical engineering from Northwestern Polytechnical University, Xi'an, China, in 2008, 2011, and 2015, respectively. From 2011 to 2014, he was a Visiting Scholar with the Department of Electrical and Computer Engineer, University of Michigan, Dearborn. In 2016, he has joined the Faculty of Vehicle Engineering, Beijing Institute of Technology, Beijing, China. His research interests include wireless power transfer, resonant power conversion, and electric motor drive for electric vehicles.

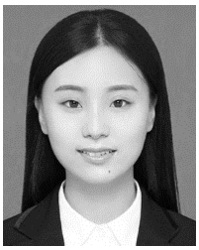

NA FU received the B.S. degree in measurement and control technology and instrumentation from the Hebei University of Technology, Tianjin, China, in 2016, and the M.S. degree in optical engineering from Beihang University, Beijing, China, in 2019. She is currently pursuing the Ph.D. degree in mechanical engineering with the National Engineering Laboratory for Electric Vehicles, Beijing Institute of Technology, Beijing. Her main research interests include wireless power transfer and electric motor drive for electric vehicles.